RSC Advances

PAPER

View Article Online
View Journal | View Issue

Cite this: *RSC Adv.*, 2025, **15**, 24872

The Mn_3O_4/biochar composite prepared from straw biochar and divalent manganese: investigation of synthetic conditions and malachite green degradation

Jianpo Zhang, * Tianqi Wang, He Gao, Yuan Gao and Li Jin *

Received 10th May 2025
Accepted 9th July 2025

DOI: 10.1039/d5ra03281d

rsc.li/rsc-advances

In this study, the goal was to recycle and reuse manganese in wastewater by use of a cheap material biochar, ammonia, and hydrogen peroxide to produce a Mn_3O_4/biochar composite, which could be used for the degradation of dye in wastewater (MG has been selected as a candidate dye mode here). The experiment condition of was optimized, and Mn_3O_4/biochar composite has been characterized by TEM, XRD, XPS and N_2 adsorption–desorption. The kinetics and isotherm of malachite green (MG) degradation were well described by the pseudo-second-order and pseudo-first-order kinetic modes, indicating that as prepared MBC both have good adsorption and photocatalytic capacity due to its component of biochar and Mn_3O_4. The maximum MG degradation capacity of MBC is 248.0 mg g^{-1}, which has a significant advantage compared with single biochar (160.9 mg g^{-1}). Above all, straw biochar, an agricultural waste product, has been used to recycle industrial heavy metal, which achieves the goal of "the method of waste control by waste".

1 Introduction

The heavy metals in high-salinity wastewater generated by chemical plants or laboratories are mostly mutagenic, teratogenic, and carcinogenic substances. If they are directly discharged into sewers or environmental water bodies without treatment, the accumulation of harmful substances over a long period can cause serious harm to the surrounding water sources, atmosphere, soil, and other environments.[1–5]

The manganese in wastewater mainly comes from textile, printing and dyeing, papermaking, steel, and smelting. Manganese primarily exists in the form of divalent manganese ions in water. Excessive manganese could result in water quality deterioration, the unfavorable smell and environmental pollution. Although manganese is one of the essential trace elements for the human body, excessive divalent manganese or long-term exposure to high concentrations of manganese may lead to chronic manganese poisoning. Because manganese can selectively inhibit the dopaminergic system of the central nervous system, causing degeneration and necrosis of nerve cells, and even Parkinson's syndrome and toxic psychosis. In addition, divalent manganese can bind to β1 globulin in the blood and accumulate in cells of the liver, kidneys, pancreas, heart, lungs, and brain, resulting in liver dysfunction, kidney damage, and pancreatic dysfunction.[6–10]

In order to protect the environment and human health, countries have established discharge standards for manganese content in wastewater. In China, the "wastewater discharge standards" (GB 8978-1996) stipulate that the manganese discharge concentration in industrial wastewater shall not exceed 1.0 mg L^{-1}, and the manganese discharge concentration in domestic wastewater shall not exceed 0.5 mg L^{-1}. Compared with China, some countries have stricter standards for manganese in wastewater. For example, the US Environmental Protection Agency (EPA) has set a manganese limit of 0.05 milligrams per litre for industrial wastewater and 0.02 milligrams per litre for domestic wastewater. These standards are based on scientific research on manganese toxicity and assessment of environmental capacity, aimed at ensuring that wastewater discharge does not have unacceptable impacts on the environment and human health. On the one hand, manganese containing wastewater can cause environmental pollution and impact on the ecological environment. On the other hand, manganese ions in wastewater containing manganese are an essential resource that can be recycled and reused to reduce resource waste.

Manganese oxides, especially manganese trioxide, as a stable oxide of transition metal manganese, have wide application value in electrochemistry, molecular adsorption, catalysis, solar energy conversion, ion exchange, and high-density magnetic storage.[11–14] It is of great significance to convert manganese wastewater into manganese trioxide for environmental protection and resource recovery.

School of Chemical and Pharmaceutical Engineering, Jilin Institute of Chemical Technology, Jilin 132022, China. E-mail: canoe8013@126.com; zhangjp725@126.com

At present, the recovery methods of manganese ions from manganese wastewater mainly include chemical oxidation, physical adsorption, ion exchange, and microbial adsorption methods.[15–19] The chemical oxidation method is suitable for low concentration of manganese ion, which has drawbacks such as high usage of chemicals and difficulty in treating wastewater. The physical adsorption method is also suitable for low concentration manganese ions. Various adsorbents such as activated carbon, silica, and ion exchange resins can be used to adsorb manganese ions onto the adsorbents, and then recover manganese ore through methods such as pyrolysis or leaching. The ion exchange method is suitable for high concentration manganese ions, which could separate manganese ions from other ions, and achieve the recovery of manganese ions. Both physical adsorption and ion exchange method have drawbacks such as low recovery rates and susceptibility to secondary pollution caused by adsorbents or resins. The microbial adsorption method is suitable for high concentration of manganese ions, which can separate manganese ions from wastewater through microbial adsorption. However, this method also has certain drawbacks, such as the harsh growth conditions of microorganisms and the difficulty of operation.

In this research, biochar with large specific surface areas has been used as adsorption carriers to adsorb divalent manganese onto/in its surface. By sequentially adding ammonia water and hydrogen peroxide, divalent manganese is converted into manganese trioxide to form Mn_3O_4/biochar composite (MBC), of which preparation conditions have been optimized. Investigations show that MBC exhibits strong signals for both $^{\cdot}O_2^-$ and $^{\cdot}OH$ radicals, which could be use as a photocatalytic degradation material. Malachite green is selected as a pollutant model to evaluate the adsorption and photocatalytic degradation properties of the synthesized material. The leaching of manganese from MBC solution has been studied to investigate the long-term stability of MBC.

Although studies have shown that it has good effects on agricultural and forestry waste to adsorb heavy metals in water,[20] which may increase the chemical oxygen demand of water bodies. This study uses inexpensive straw organisms as the primary raw material, which not only achieves the recycling and reuse of manganese in manganese wastewater, but also efficiently removes dye pollutants from water bodies, which is one of the effective ways to solve agricultural waste and achieve the goal of "the method of waste control by waste".

2 Experimental

2.1 Materials and reagents

Ultrapure water, manganese sulfate (>99%, Beijing Chaoyang District chemical plant No. 4), hydrogen peroxide (35%, Tianjin Yongda chemical reagent factory), ammonium hydroxide (25%, Tianjin Damao chemical reagent factory), straw biochar (biochar in short), malachite green (Tianjin Hedong District red rock reagent factory). All other agents were of analytical reagent grade and used as received. Water used throughout was doubly distilled water (>18 MΩ cm).

2.2 Instrumentation and spectrometry

The transmission electron micrographs (TEM) were recorded with a JEM-F200 electron microscope. Powder X-ray diffraction (PXRD) patterns were collected on a Malvern Panalytical B.V Empyrean X-ray diffractometer with graphite monochromatized Cu Kα radiation (λ = 0.154 nm, U = 45 kV, I = 40 mA) and 2θ ranging from 10° to 80° with an increment of 0.02° and a scanning rate of 5° min^{-1}. The XPS spectra were recorded with a Scientific K-Alpha. The TG-DSC were recorded with a Discovery SDT650.

2.3 The preparation of MBC

1.5 g of manganese sulfate was added and dissolved in 100 mL distilled water. The 0.5 g biochar was added and stirred with a magnetic stirrer for 1 h. Then, 20 mL of ammonia solution was added dropwise at a speed of 5 drips per minute. After stirring for an additional 20 min, 1 mL of hydrogen peroxide was added at a speed of 15 drips per minute. After stirring for 1 hour at 60 °C, the suspensions were filtered immediately, and vacuum-dried at 60 °C for 12 h, dark brown power was obtained. Controlled experiment was adopted without adding biochar.

2.4 The degradation of MG adopted by MBC

Under magnetic stirring, the time period begins when a certain amount of MG and 0.2 g BAC are added into 100 mL deionized water, 1 mL solution is taken every 10 min. After centrifugation at 3000 rpm for 3 min, absorption spectrum of supernatant is measured by use a UV-vis spectrophotometer. Similar experiments are adopted with the condition of lucifuge, natural light, and illuminated by xenon lamp.

3 Results and discussion

3.1 Characterization of MBC

The morphology and structure characterizations of MBC are employed by high-resolution transmission electron microscopic (HRTEM), and results are shown in Fig. 1A. Results show that the morphology of MBC is irregular flake-like, and the interplaner distance of the crystalline lattice plane is 0.25 nm corresponding to Mn_3O_4,[21] indicated that Mn_3O_4 has doped on the surface of MBC. Also, as shown in Fig. 1B, the result of powder X-ray diffraction (XRD) pattern corresponding to the typical planes of Mn_3O_4 (Pdf no. 24-0734),[22] which is consistent with the result of HRTEM. XPS result (Fig. 1C) shows that there are C, O, and Mn elements in the as-prepared MBC. As shown in Fig. 1D, the distance between the Mn $2p_{3/2}$ peak at 641.2 eV and the Mn $2p_{1/2}$ peak at 652.7 eV is ~11.5 eV, which is characteristic of Mn^{3+}.[23,24] Furthermore, the Mn $2p_{3/2}$ peak was analysed by software of XPS peak 41, and can be deconvoluted using three Gaussian components (Fig. 2A), which correspond to Mn^{2+} at 640.4 eV, Mn^{3+} at 641.7 eV and Mn^{4+} at 642.7 eV.[25] The percentages of manganese in three valence states are calculated, based on the ratios of three peak integral areas under the curve from Fig. 2A, and the average valence state of Mn in MBC is about 2.93, which is similar to the average valence state of Mn (2.67) in Mn_3O_4. Furthermore, as shown in Fig. 2C, the peak at

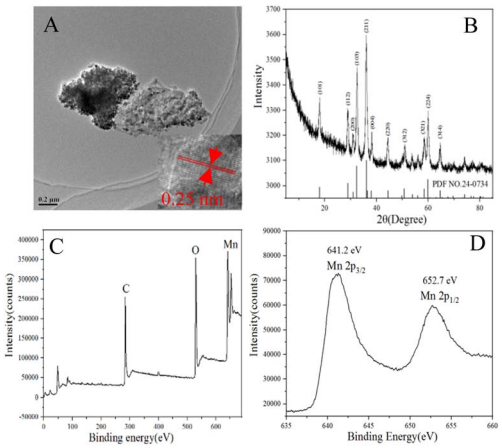

Fig. 1 TEM images (A), XRD (B), XPS survey (C) of MBC, high resolution XPS (D) of Mn 2p.

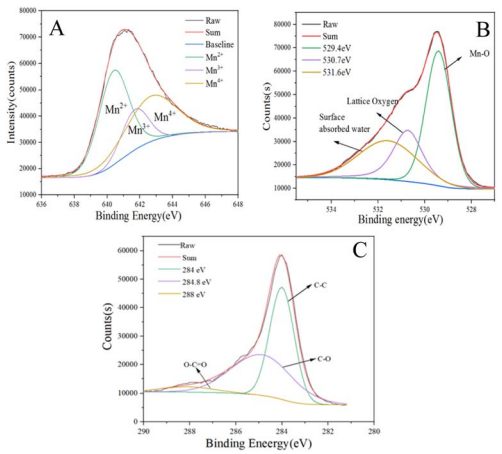

Fig. 2 High resolution XPS spectra of $Mn2p_{3/2}$ (A), O1s (B) and C1s (C).

530.7 eV in the O1s peak is correspond to lattice oxygen, and the peak at 529.4 eV in the O1s peak is correspond to Mn–O. Furthermore, as shown in Fig. 2C, the peak at 284 eV in the C1s peak is correspond to C–C, the peak at 284.8 eV in the C1s peak is correspond to C–O, and the peak at 288 eV in the C1s is corresponding to O–C=O. All data indicate that MBC has been successfully synthesized.

3.2 The optimization of MBC preparation conditions

To get good performance Mn_3O_4 doped material, reaction conditions have been optimized. As shown in Fig. 3A, when the ratios of biochar to $MnSO_4$ varied from 1 : 1 to 1 : 3 (lines *a*, *b*, *c* in Fig. 3A), the diffraction peak at 19° shifted gradually to 18°, and the peaks at 58.5° and 69.8° intensified. The peak at 19° corresponds to MnO_2 (Pdf no. 12-0141, in Fig. 3B), the peak at 18° corresponds to Mn_3O_4 (Pdf no. 24-0734). When the ratios of biochar to $MnSO_4$ reached 1 : 3 (line *c* in Fig. 3A), the XRD peaks of MBC match perfectly with the standard Mn_3O_4 peaks. When the ratios of biochar to $MnSO_4$ varied from 2 : 7 to 1 : 4 (lines *d*, *e* in Fig. 3A), the diffraction peak at 19° reappears, and the peaks

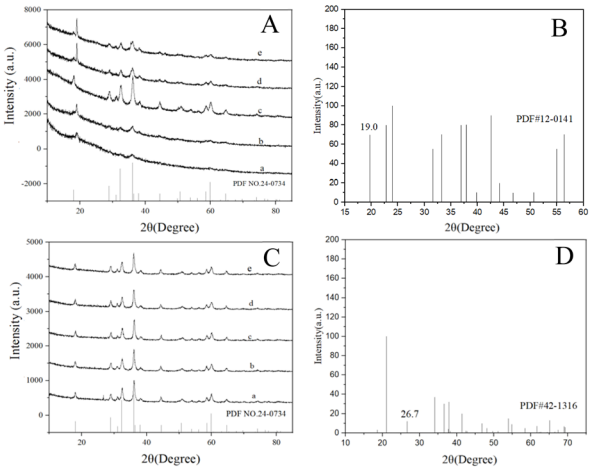

Fig. 3 The effect of the mass ratios of biochar to $MnSO_4$ (A), stirring time (C) on the XRD of MBC, and the standard XRD of MnO_2 (B and D). (The mass ratios of biochar to MnSO4 are 1 : 2, 2 : 5, 1 : 3, 2 : 7, and 1 : 4. The stirring times are 0.5, 1, 2, 3, 4 h).

at 58.5° and 69.8° gradually decrease. This is because Mn^{2+} has been over-oxidized to MnO_2 by hydrogen peroxide and atmospheric oxygen, when the ratios of biochar to $MnSO_4$ is at 1 : 2 and 2 : 5. When excessive Mn^{2+} is added, it is not quick enough for the Mn^{2+} to be oxidized, induce the formation of MnO. So, the mass ratio of biochar to manganese sulfate of 1 : 3 is selected.

The stirring time also significantly influenced the divalent manganese ions removing efficiency of biochar (Fig. 3C). When the stirring time is 0.5 h, a peak appeared at 26.7° is the characteristic peak of MnO_2 (Pdf no. 42-1316, in Fig. 3D), indicates over oxidation of Mn^{2+}. When the stirring time reaches 1 hour, the XRD peaks of MBC match perfectly with the XRD peaks of Mn_3O_4 at $2\theta = 18.2°$, 28.9°, 32.8°, 36.2°, and 60.2°. But peak at 26.7° will appear after stirring over 3 h, indicating over-oxidation of the surface manganese. So, the optimal stirring time of 1 h for manganese ion adsorption by biochar is selected.

The effect of the drip speeds and dosages of ammonia on the formation of manganese hydroxide from divalent manganese adsorbed on biochar have been discussed, and corresponding results were shown in Fig. 4. As shown in Fig. 4A, when the dropping speeds are too fast (line *b*–*e*), double peaks at 18° and 19° appear, due to incomplete oxidation of internal $Mn(OH)_2$. So, drip speed of 5 drips per minute is selected.

As shown in Fig. 4B, when the doses of NH_3 H_2O are more than 2.67 mol L^{-1}, the peaks of MBC match perfectly with the XRD peaks of Mn_3O_4, and remain relatively unchanged along with the increasing of NH_3 H_2O doses. This is because that insufficient ammonia dosage will be led to over oxidization of Mn^{2+} to MnO_2, which is consistent to the characteristic peak of standard MnO_2 at 26.7° (Pdf no. 42-1316, in Fig. 4C). So, the NH_3 H_2O dosage of 2.67 mol L^{-1} is selected.

In the reaction, manganese(II) oxide is oxidized to manganese(II) oxidized (from $Mn(OH)_2$ to Mn_3O_4) by both hydrogen peroxide and oxygen from the air. So, the drip speeds and dosages of hydrogen peroxide have significant effect on the

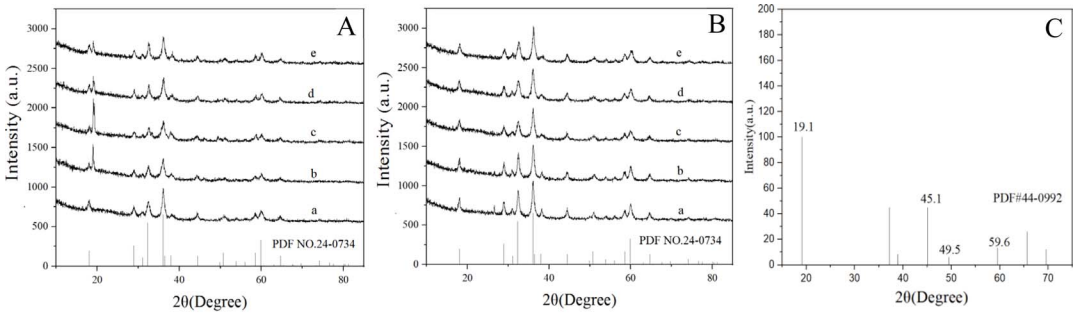

Fig. 4 The effect of the dropping speeds (A) and dosages (B) of NH_3 H_2O added on the XRD of MBC, the standard XRD of MnO_2 (C). (The dropping speeds are 5, 10, 15, 20 and 25 drip per minute. The dosages are 1.34, 2.00, 2.67, 3.34 and 4.01 mol L^{-1}).

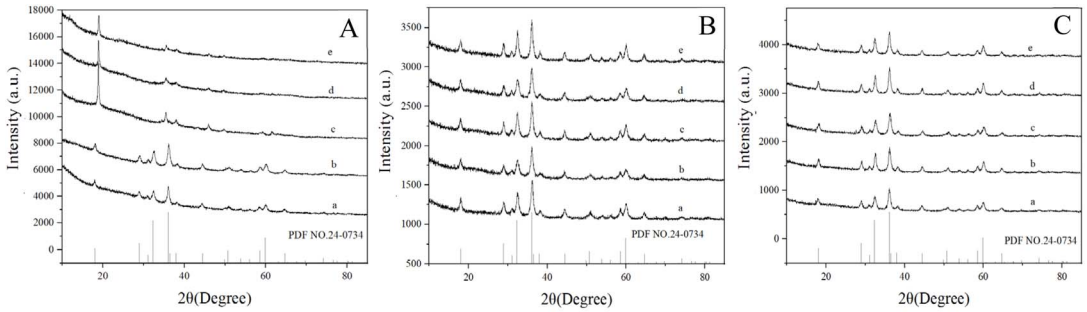

Fig. 5 The effect of the dosages (A) and dropping speeds (the presence or absence of oxygen, B and C) of H_2O_2 added on the XRD of MBC. (The dosages are 0, 0.10, 1.0, 1.5 and 2.0 mol L^{-1}, the dropping speeds are 5, 10, 15, 20 and 25 drip per minute).

formation of Mn_3O_4 on the product. As shown in Fig. 5A, the optimal dosage of hydrogen peroxide added is 0.1 mol L^{-1}. When the dosages of hydrogen peroxide exceed 1 mL (lines *c*, *d*, *e*), the characteristic peaks of MnO_2 appeared at 19.0°, 45.9°, 49.6°, and 59.2°, consistent with Pdf no. 44-0992 (shown in Fig. 5C), due to over oxidization of $Mn(OH)_2$ by hydrogen peroxide.

Under the presence or absence of oxygen condition, the effect of drip speeds of H_2O_2 on the XRD of MBC are shown in Fig. 5B and C, which shown that the optimal drip speed is 15 drips per min with the presence of oxygen. Because catalytic decomposition of the H_2O_2 adopted by Mn^{2+} would occur, when the drip speed is too lowly. And over oxidization of $Mn(OH)_2$ would occur, when the drip speed is too fast. Furthermore, compared with Fig. 5A–C XRD peaks of MBC at 18°, 28.8°, 32.5°, 36.0°, 58.6°, and 60.0° were closer to the standard card of Mn_3O_4. Therefore, the optimal H_2O_2 drip rate at 15 drips per min in the presence of oxygen is selected. Above all, the optimal conditions for synthesis are the ratio of biochar to $MnSO_4$ is 1 : 3, the dosage and drip speed of NH_3 H_2O is 2.67 mol L^{-1} and five drips per minute, the dosage and drip speed of hydrogen peroxide is 0.1 mol L^{-1} and 15 drips per min, respectively. We can conclude that biochar could adsorb Mn^{2+} in industrial wastewater to synthesize the MBC.

As shown in Fig. 6A, both the nitrogen adsorption–desorption isotherm of biochar and MBC show type IV isotherm, indicating that pore size of biochar and MBC are in the range of mesopore. The Brunauer–Emmett–Teller (BET) surface area of

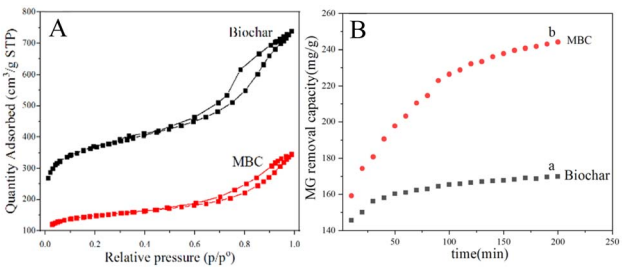

Fig. 6 Isotherm linear plot of biochar and MBC (A), and the removal capacities of MG by biochar and MBC under nature light (B).

Table 1 Comparison of different degradation materials

Material	Time (min)	Degradation percentage
NFO-700	120	99%
$Au/NaNbO_3$	40	100%
EDTA modified ZnO	40	94.14%
$KMnO_4$ modified bichar	120	99%
Cu_2ZnSnS_4	150	76%
MBC	40	99.35%

biochar and MBC are about 1364.3 and 551.5 m^2 g^{-1}, respectively. The BJH adsorption cumulative volume of pore between 1.7 nm and 297.8 nm diameter of biochar and MBC are 0.7576

and 0.3808 $cm^3\ g^{-1}$, and BJH desorption cumulative volume of pore between 2.0 nm and 300.0 nm diameter of biochar and MBC are 0.7353 and 0.3767 $cm^3\ g^{-1}$. Results above show that adsorption ability of biochar is significantly better than that of MBC. Because the pores in biochar are filled or covered by Mn_3O_4, which is doped in/on the biochar. Because the size of dye is about 2.57 nm,[25] MG could be easily adsorbed in the mesoporous shell, because the adsorption and desorption average pore diameter (4V/A by BET) are 3.347 and 3.868 nm, respectively. MG could be adsorbed quickly on MBC due to the high surface area and a large number of mesoporous on the surface.

3.3 MG degradation mechanism of MBC

To evaluate the dye removal capacity of MBC, MG is selected as a candidate, and biochar is selected as a control. The MG removal capacity comparison of biochar and MBC under similar condition are shown in Fig. 6B. As shown in Fig. 6B, the equilibrium amount of MG removed by biochar and MBC are 160.9 and 248.0 mg g^{-1}, respectively, which shows that MBC has better removal capacity than biochar, due to the Mn_3O_4 in/on the MBC. Compared with other materials, MBC has advantage in degradation time and rate, as shown in Table 1.

To prove that Mn_3O_4 in/on the MBC is important and has significant effect on the removal of MG in solution, the MG removal capacities by MBC were studied under the conditions of lucifuge, natural light, and illuminated by xenon lamp (Fig. 7A). MBC with illuminating by xenon lamp has significant advantage on the MG removal capacity and the equilibrium time, compared with the conditions of lucifuge and natural light. The corresponding data were then analysed by the pseudo-second-order (Fig. 7B) and pseudo-first-order kinetic modes (Fig. 7C), and relevant eqn (1) and (2) are shown below, and calculation results are shown in Fig. 7 and Table 2.

$$\frac{t}{q_t} = \frac{1}{K_2 q_e^2} + \frac{t}{q_e} \quad (1)$$

$$\ln\left(\frac{C_0}{C_t}\right) = K_{app}\ t \quad (2)$$

where q_e and q_t are the amount of MG removed by MBC at equilibrium and time t, respectively. C_0 and C_t are the initial concentration of MG and the amount of MG at time t, respectively. K_2 and K_{app} are the rate constants of pseudo-second-order (g mg^{-1} min^{-1}) and pseudo-first-order kinetic modes (1/min).

Table 2 Comparison of the different kinetic model parameters from Fig. 7B and C

	Second-order-kinetic model			First-order-kinetic model	
	q_e	k_2(g mg^{-1} min^{-1})	R^2	k_{app}(/min)	R^2
Lucifuge	507.6	7.520×10^{-4}	0.9980	0.01760	0.9896
Natural light	510.2	7.753×10^{-4}	0.9984	0.01432	0.9981
Illumination	531.9	7.864×10^{-4}	0.9995	0.01797	0.6665

All data from Fig. 7 fit well with the second-order-kinetic model, of which R^2 are 0.9980, 0.9984, and 0.9995, respectively. Data are then analysed by pseudo-first-order kinetic modes, of which results are different. Date from natural light condition both fits pseudo-second-order (R^2 is 0.9984) and pseudo-first-order kinetic modes (R^2 is 0.9896), and corresponding k_{app} (0.01432 min^{-1}) is significantly faster than that of k_2 (7.753×10^{-4} g mg^{-1} min^{-1}), which indicates that the removing progress undergoes both adsorption and photocatalytic degradation progress, and the rate of photocatalytic degradation progress is significantly faster than that of the adsorption progress. As it is well known that rate-determining step (RDS) is the slowest step, so the adsorption step is the rate determine step for MG removing by MBC. When the MG removing progress is adopted under illuminating by xenon lamp condition, the illumination could further accelerate photocatalytic degradation rate, MG are degraded as soon as adsorbing on the MBC, so this removing progress could quickly reach equilibrium. This may be why data from illumination condition only fits well with second-order-kinetic mode (R^2 is 0.9995), and the poor pseudo-first-order fit under illumination ($R^2 = 0.6665$).

To investigate the photocatalytic degradation mechanism, electron paramagnetic resonance (EPR) spectroscopy was employed, which show that MBC exhibits strong signals for both $^{\bullet}OH$ (Fig. 8A) and $^{\bullet}O_2^-$ (Fig. 8B) radicals. The photocatalytic degradation mechanism could be explained as follows. As Li and Khan[26] reported Mn_3O_4 can absorb light energy and

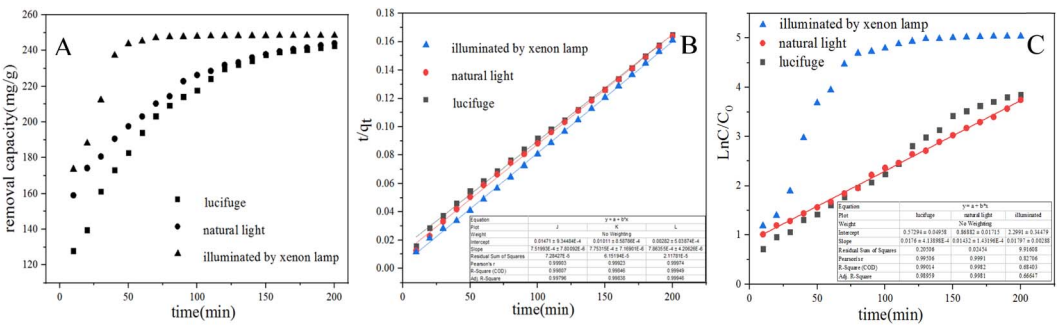

Fig. 7 The effect of lucifuge, natural light and illuminated by xenon lamp on the removal capacities of MG by MBC (A), data were fitted by pseudo-second-order (B) and pseudo-first-order modes (C).

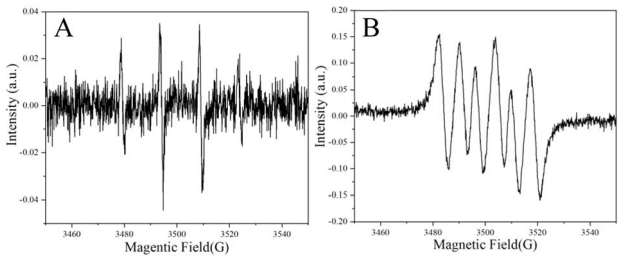

Fig. 8 Situ EPR spectra for detection of $^{\bullet}OH$ (A) and $^{\bullet}O_2^-$ (B) radicals under light illuminate.

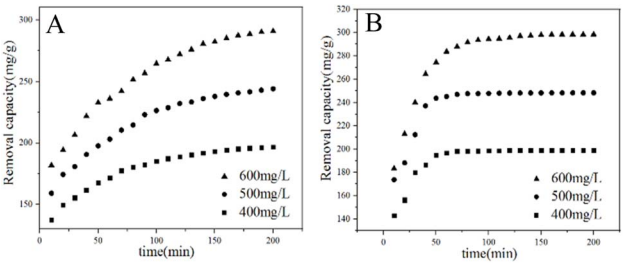

Fig. 10 The MG removal capacities of MBC under natural light (A) and illuminated by xenon lamp (B).

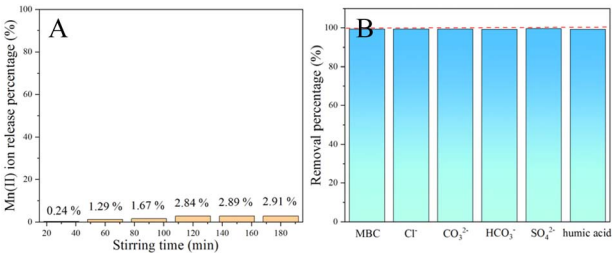

Fig. 11 The Mn(II) ion release percentage at different stirring time (A), the influence of some common wastewater components on MG degradation by MBC.

excite electrons to produce excited electrons (e^-) and holes (h^+) under light conditions. These excited electrons and holes can participate in subsequent redox reactions. Excited electrons react with dissolved oxygen to form superoxide anions ($\cdot O_2^-$) or hydrogen peroxide (H_2O_2), while holes react with water to form hydroxyl radicals ($\cdot OH$). These active species have a strong oxidation capacity to dye, so Mn_3O_4 plays an essential role in the photocatalytic degradation of MG. So, it is why data from lucifuge condition only fits well with adsorption progress under the (R^2 is 0.9980), photocatalytic degradation could not occur without light. We can conclude that as prepared MBC both have good adsorption and photocatalytic capacity due to its component of biochar and Mn_3O_4.

3.4 Effect of MBC concentration on MG removing

It is importance to optimize the MBC concentration for effective MG removing. To determine the optimized MBC concentration for the photocatalytic degradation of MG, different concentration of MBC (from 0.5–4 g L^{-1}) were added into fixed concentration MG solutions. As shown in Fig. 9, the removal percentage increases along with concentration increasing of MBC, and then reaches equilibrium after the concentration of MBC is more than 2 g L^{-1}. Also, Li[27] has reported that too much catalyst may prolong time due to competition between catalyst and dye molecule for active sites. So, the MBC concentration of 2 g L^{-1} is selected for further study.

The removing capacity and equilibrium time are also affected by the concentrations of MG. The comparation of MG removal capacities of MBC of two reaction conditions are shown in Fig. 10, which show similar results with Fig. 7A. Illuminating by xenon lamp could significantly accelerate the MG degradation reaction rate. Furthermore, the more the initial concentration of MG (from 400 mg L^{-1} to 600 mg L^{-1}), the more equilibrium time is needed, and the more MG is removed by MBC. Because the higher initial MG concentration provides, the more powerful driving force for MG to diffuse from the solution to the surface of MBC, resulting in faster photocatalytic degradation of MG by Mn_3O_4 doped in the MBC.

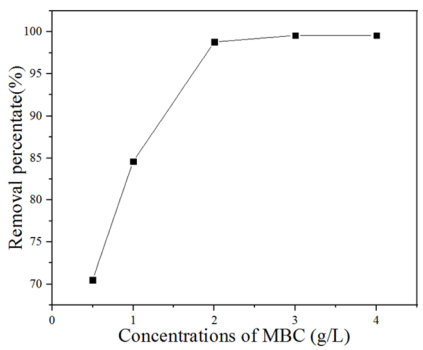

Fig. 9 Optimization of the MBC concentration for removing MG. (The concentration of MG is 600 mg L^{-1}).

3.5 The stability and influence experiment of MBC

To investigate the long-term stability of MBC, the leaching of manganese of MBC in solution has been studied. 0.2 g MBC was dissolved in 30 mL water under continue stirring, and 2 mL solution was taken at different stirring times. The Mn(II) ion release percentage was detected through periodic acid oxidation method. As shown in Fig. 11A, after stirring for 3 h, the Mn(II) ion release percentage was only 2.91%, indicates that MBC has a good long-term stability in water solution. Also, the effect of some common wastewater components (Cl^-, SO_4^{2-}, CO_3^{2-}, HCO_3^- and humic acid) on MG degradation by MBC has been studied and shown in Fig. 11B. Results show that the effect of these interfering substances is difficult to be distinguished. Above all, MBC has good stability and anti-interference ability.

4 Conclusion

Mn_3O_4/biochar composite has been successfully synthesized through co-precipitation and hydrogen peroxide oxidation. The

effect of the stirring time, mass ratios, dropping speeds and dosages of NH_3 H_2O and H_2O_2 on the XRD analysis of MBC have been discussed seriously to get good performance product. And the optimal conditions for synthesis are the ratios of biochar to $MnSO_4$ is 1 : 3, the dosage and drip speed of NH_3 H_2O is 2.67 mol L^{-1} and 5 drips per minute, the dosage and drip speed of hydrogen peroxide is 0.1 mol L^{-1} and 15 drips per min, respectively. Furthermore, MG is selected as a candidate to evaluate the dye removal capacity of MBC, of which degradation mechanism discussed through the pseudo-second-order and pseudo-first-order kinetic modes indicates that MBC both have good adsorption and photocatalytic capacity. So, manganese has been recycled by straw biochar to form a Mn_3O_4/biochar composite, which could be used in dye wastewater treatment.

Data availability

The data are available from the corresponding author on reasonable request.

Author contributions

Jianpo Zhang: corresponding author, theoretical direction. Tianqi Wang: editing – original draft, investigation. He Gao and Yuan Gao: data curation. Li Jin: corresponding author, conceptualization, methodology, funding acquisition, writing – review, supervision.

Conflicts of interest

There are no conflicts to declare.

Acknowledgements

This work is supported by the department of Science and Technology of Jilin Province (20240101165JC). XRD data were obtained using equipment maintained by Jilin Institute of Chemical Technology Center of Characterization and Analysis. The authors would like to thank Linghui Bu from Shiyanjia Lab (**www.shiyanjia.com**) for the TEM, and XPS analysis.

References

1 L. X. Li, J. Z. Han, L. L. Huang, L. L. Liu, S. Qiu, J. Ding, X. H. Liu and J. Zhang, Activation of PMS by MIL-53(Fe) @AC composites contributes to tetracycline degradation: properties and mechanisms, *Surf. Interfaces*, 2024, **51**, 104521.

2 S. Shokri, B. Bonakdarpour and E. A. Sharghi, How high salt shock affects performance and membrane fouling characteristics of a halophilic membrane bioreactor used for treating hypersaline wastewater, *Chemosphere*, 2024, **354**, 141716.

3 C. Deng and G. M. Weng, A multifunctional device for simultaneous hypersaline wastewater desalination, waste acid-base neutralization, and electricity generation, *Nano Energy*, 2024, **126**, 109674.

4 L. X. Li, S. Li, X. J. Ke, D. Dong and L. Huang, Anammox in treatment of coal chemical wastewater: a review, *J. Min. Sci. Technol.*, 2025, **10**(2), 351–362.

5 F. Quan, G. Zhan, P. Xu, X. F. Chen, X. L. Chen, W. J. Shen and F. L. Jia, Electrochemical removal of nitrate in high-salt wastewater with low-cost iron electrode modified by phosphate, *J. Environ. Sci.*, 2025, **148**, 38–45.

6 L. X. Li, T. J. Liang, M. J. Zhao, Y. Lv, Z. W. Song, T. Sheng and F. Ma, A review on mycelial pellets as biological carriers: Wastewater treatment and recovery for resource and energy, *Bioresour. Technol.*, 2022, **355**, 127200.

7 T. L. Gerke, B. J. Little and M. J. Barry, Manganese deposition in drinking water distribution systems, *Sci. Total Environ.*, 2016, **541**, 184–193.

8 C. Marchetti, Role of calcium channels in heavy metal toxicity, *ISRN Toxicol.*, 2013, **3**, 184360.

9 T. V. Peres, M. R. C. Schettinger, P. Chen, F. Carvalho, D. S. Avila, A. B. Bowman and M. Aschner, Manganese-induced neurotoxicity: a review of its behavioral consequencesand neuroprotective strategies, *MBC Pharmacol. Toxicol.*, 2016, **17**(1), 57.

10 L. Yin, Q. J. Dai, P. P. Jiang, L. Zhu, H. F. Dai, Z. J. Yao, H. Liu, X. P. Ma, L. X. Qu and J. K. Jiang, Manganese exposure facilitates microglial JAK2-STAT3 signaling and consequent secretion of TNF-a and IL-1β to promote neuronal death, *Neurotoxicology*, 2018, **64**, 195–203.

11 S. Anu, C. Malathi, N. Lakshmi, S. M. Adalagere, P. R. Deepthi, V. A. Jagadeesha, P. M. Kumar and P. Mehaboob, Synthesis, phase transformation, and morphology of hausmannite Mn_3O_4 nanoparticles: photocatalytic and antibacterial investigations, *Heliyon*, 2020, **6**(1), e03245.

12 M. Jayandran, M. M. Haneefa and V. Balasubramanian, Green synthesis and characterization of manganese nanoparticles using natural plant extracts and its evaluation of antimicrobial activity, *J. Appl. Pharm. Sci.*, 2015, **5**(12), 105–110.

13 Y. Li, Y. H. Li, Z. T. Zhang, X. H. He and J. L. Chen, Preparation of Mn_3O_4 by precipitation conversion-roasting method and its morphological evolution, *Ceram. Int.*, 2021, **47**(16), 21570–21575.

14 Z. J. Yi, W. Li, B. Xiao, W. Q. Zhang, Y. C. Xiong, Y. B. Luo, Q. H. Jiang, X. Li and J. Y. Yang, Ecofriendly Mn_3O_4 as a novel hole transport material for efficient and ultrastable flexible and rigid perovskite solar cells, *ACS Sustain. Chem. Eng.*, 2023, **11**(35), 13232–13239.

15 K. Vijayaraghavan and Y. S. Yun, Bacterial biosorbents and biosorption, *Biotechnol. Adv.*, 2008, **26**(3), 266–291.

16 S. Vishali, and E. Kavitha, Chapter 6 – Application of membrane-based hybrid process on paint industry wastewater treatment, *Membrane-Based Hybrid Processes for Wastewater Treatment*, Elsevier, 2021, pp. 97–117.

17 A. Mavhungu, V. Masindi, S. Foteinis, K. K. R. Mbaya and E. Chatzisymeon, Advocating circular economy in wastewater treatment: Struvite formation and drinking water reclamation from real municipal effluents, *J. Environ. Chem. Eng.*, 2020, **8**(4), 103957.

18 N. N. Rudi, M. S. Muhamad, T. C. Lee, J. Alipald, S. Omara, N. Hamidon, N. H. A. Hamid, N. M. Sunar, R. Alib and H. Harun, Evolution of adsorption process for manganese removal in water *via* agricultural waste adsorbents, *Heliyon*, 2020, **6**(9), 5049.

19 M. A. Acheampong, R. J. W. Meulepas and P. N. L. Lens, Removal of heavy metals and cyanide from gold mine wastewater, *J. Chem. Technol. Biotechnol.*, 2010, **85**(5), 590–613.

20 P. Chand and Y. B. Pakade, Removal of Pb from water by adsorption on apple pomace: Equilibrium, kinetics, and thermodynamics studies, *J. Chem.*, 2013, **2013**, 1–8.

21 C. C. Huang, N. H. Khu and C. S. Yeh, The characteristics sub 10 nm manganese oxide T_1 contrast agents of different nanostructured morphologies, *Biomaterials*, 2010, **31**, 4073–4078.

22 H. Hu, A. Dai, J. Sun, X. Y. Li, F. H. Gao, L. Z. Wu, Y. Fang, H. L. Yang, H. An, X. Wu and S. P. Yang, Aptamer-conjugated Mn_3O_4@SiO_2 core-shell nanoprobes for targeted magnetic resonance imaging, *Nanoscale*, 2013, **5**, 10447–10454.

23 S. Ardizzone, C. L. Bianchi and D. Tirelli, Mn_3O_4 and γ-MnOOH powders, preparation, phase composition and XPS characterization, *Colloids Surf., A*, 1998, **134**(1), 305–312.

24 V. D. Castro and G. Polzonetti, XPS study of MnO oxidation, *J. Electron Spectrosc.*, 1998, **48**(1), 117–123.

25 N. Li, Y. Tian, J. Zhao, J. Zhang, J. Zhang, W. Zuo and Y. Ding, Efficient removal of chromium from water by Mn_3O_4@ZnO/Mn_3O_4 composite under simulated sunlight irradiation: Synergy of photocatalytic reduction and adsorption, *Appl. Catal., B*, 2017, **214**, 126–136.

26 S. Khan, A. Hussain, K. He, *et al.*, Tailoring the bandgap of Mn3O4 for visible light driven photocatalysis, *J. Environ. Manage.*, 2021, **293**, 112854.

27 L. L. Lian, X. L. Cao, Y. Q. Wu, D. W. Lou and D. D. Han, Synthesis of organo-functionalized magnetic microspheres and application foranionic dye removal, *J. Taiwan Inst. Chem. Eng.*, 2013, **44**, 67–73.